BIOCHEMISTRY
including biophysical chemistry & molecular biology

Article

pubs.acs.org/biochemistry

An Intrinsically Disordered Region in the Proapoptotic ASPP2 Protein Binds to the *Helicobacter pylori* Oncoprotein CagA

Tali H. Reingewertz,[†,⊥] Anat Iosub-Amir,[‡] Daniel A. Bonsor,[†] Guy Mayer,[‡] Hadar Amartely,[‡] Assaf Friedler,[‡] and Eric J. Sundberg*[,†,§,∥]

[†]Institute of Human Virology, [§]Department of Medicine, and [∥]Department of Microbiology and Immunology, University of Maryland School of Medicine, Baltimore, Maryland 21201, United States

[‡]Institute of Chemistry, The Hebrew University of Jerusalem, Jerusalem 91904, Israel

Supporting Information

ABSTRACT: The leading risk factor for gastric cancer in humans is infection by *Helicobacter pylori* strains that express and translocate the oncoprotein CagA into host epithelial cells. Once inside host cells, CagA interacts with ASPP2, which specifically stimulates p53-mediated apoptosis and reverses its pro-apoptotic function to promote ASPP2-dependent degradation of p53. The X-ray crystal structure of a complex between the N-terminal domain of CagA and a 56-residue fragment of ASPP2, of which 22 residues were resolved, was recently described. Here, we present biochemical and biophysical analyses of the interaction between the additional regions of CagA and ASPP2 potentially involved in this interaction. Using size exclusion chromatography−multiangle laser light scattering, circular dichroism, and nuclear magnetic resonance analyses, we observed that the ASPP2 region spanning residues 331−692, which was not part of the ASPP2 fragment used for crystallization, is intrinsically disordered in its unbound state. By surface plasmon resonance analysis and isothermal titration calorimetry, we found that a portion of this disordered region in ASPP2, residues 448−692, binds to the N-terminal domain of CagA. We also measured the affinity of the complex between the ASPP2 fragment composed of residues 693−918 and inclusive of the fragment used for crystallization and CagA. Additionally, we mapped the binding regions between ASPP2 and CagA using peptide arrays, demonstrating interactions between CagA and numerous peptides distributed throughout the ASPP2 protein sequence. Our results identify previously uncharacterized regions distributed throughout the protein sequence of ASPP2 as determinants of CagA binding, providing mechanistic insight into apoptosis reprogramming by CagA and potential new drug targets for *H. pylori*-mediated gastric cancer.

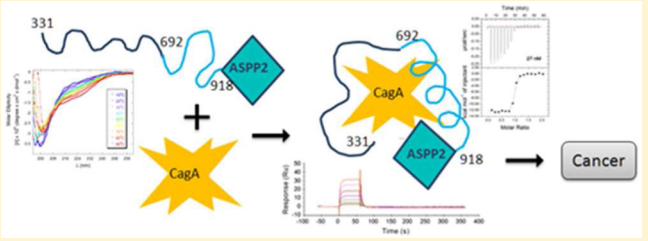

Impaired apoptosis can lead to cancer by enabling the survival of damaged cells.[1−3] Accordingly, the proteins and pathways that regulate apoptosis are targets for the development of cancer therapies.[4,5] One such protein is the apoptosis stimulating protein of p53-2 (ASPP2), which enhances the pro-apoptotic activity of p53 upon DNA damage or oncogenic stimuli.[6,7] ASPP2 binds the p53 core/DNA binding domain and enhances its transactivation function on promoters of numerous pro-apoptotic genes.[6−8] The TP53BP2 gene encodes two ASPP2 splicing variants: full-length ASPP2 (residues 1−1128) and the ASPP2 N-terminal truncated isoform, termed Bcl-2 binding protein (Bbp, residues 1−1005).[6,9,10] ASPP2 and Bbp are primarily cytoplasmic,[6,11] but Bbp is also localized, in part, within the mitochondria and induces apoptosis via the mitochondrial death pathway.[12] Downregulation of ASPP2 levels has been observed in several types of cancers,[6,9] and ASPP2 downregulation frequently correlates with poor prognoses in cancer patients.[13]

ASPP2 regulates apoptosis through additional pathways mediated by interactions with numerous proteins including the p53 family members p63 and p73,[14,15] the antiapoptotic protein Bcl-2[16] and related family members,[17] the p65 subunit of the transcription factor NF-κB,[11] protein phosphatase 1 (PP1),[18] the Hepatitis C virus (HCV) core protein,[19] and the Ras oncoprotein.[20] ASPP2 has an important role in regulating other cellular process such as cell senescence through interactions with Ras[21] or regulating cell polarity through interactions with Par-3.[22] Most of these interactions are mediated through four ankyrin repeats and an SH3 domain (Ank-SH3) in the ASPP2 C-terminal region (Figure 1A). In addition to the Ank-SH3 domains, ASPP2 contains a structured N-terminal domain with a ubiquitin-like fold (residues 1−123)[23] that mediates the ASPP2 interaction with Ras[20] and an intrinsically disordered proline (Pro)-rich domain (residues 893−918).[24,25] An intramolecular interaction between the Ank-SH3 and Pro-rich domains regulates the intermolecular interactions of ASPP2 and its apoptotic activity.[24,25] ASPP2 residue S827 in the Pro-rich domain is phosphorylated by MAPK, which leads to Ras-induced increased binding of ASPP2 to p53.[26]

Received: January 28, 2015
Revised: May 11, 2015
Published: May 12, 2015

DOI: 10.1021/acs.biochem.5b00084
Biochemistry 2015, 54, 3337−3347

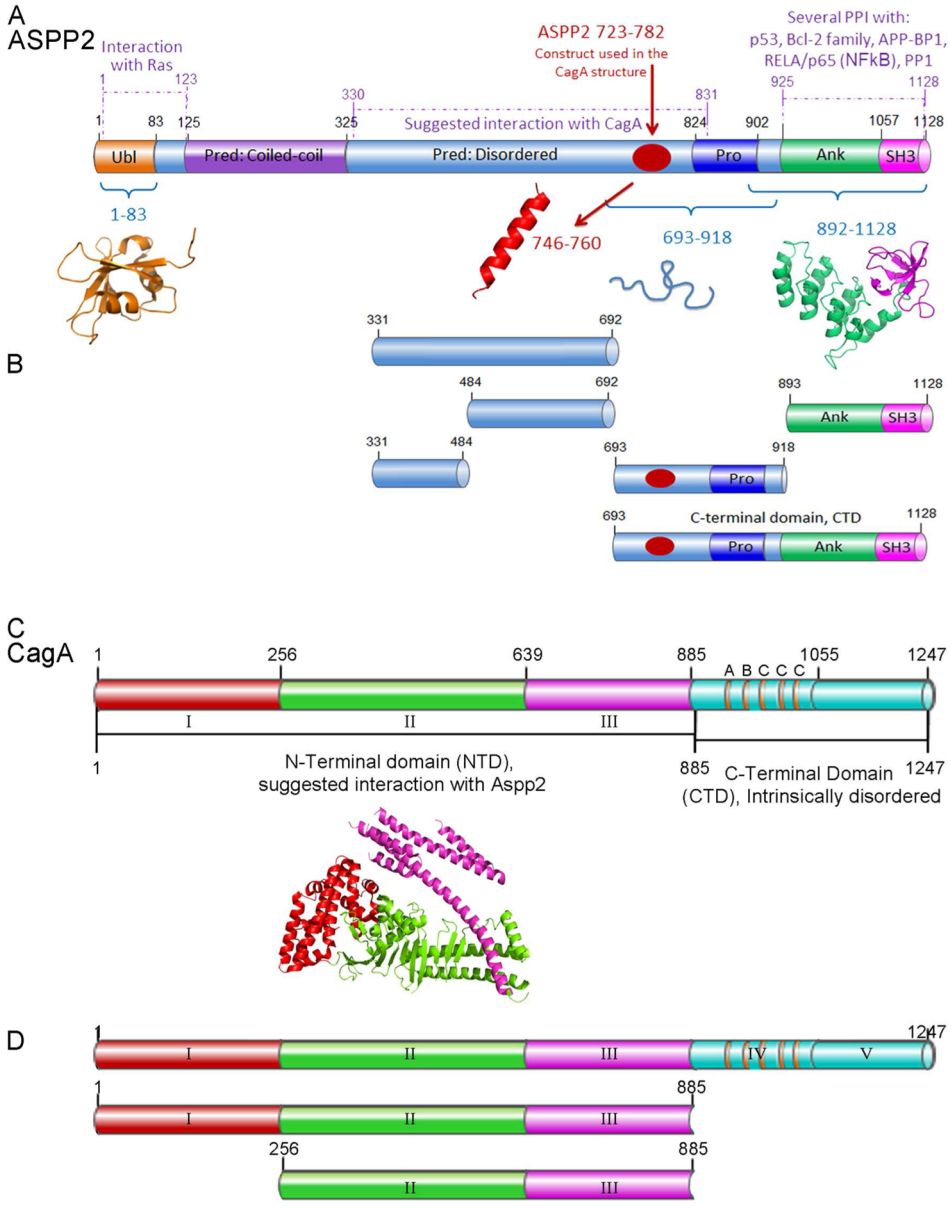

Figure 1. Schematic representation of the proteins studied. Structural organization of ASPP2 and CagA. The structures of the known domains are presented under their labels. The constructs used in this study are presented under each sequence. (A) ASPP2 domains include the following: ubiquitin-like fold (Ubl) (PDB: 2UWQ), a predicted coiled coil domain, a predicted IDR through residues 331−692, a proline-rich domain (Pro) that was experimentally determined as IDR, followed by four ankyrin repeats, and a SH3 (Ank-SH3) domain (PDB: 1YCS). Some of the known interactions mediated through the different domains are indicated in purple above the domains, including the location of the helix formed in ASPP2 Pro region in complex with domain I of CagA. (B) ASPP2 protein fragments used in this study. (C) CagA domains based on the structure from Hayashi et al.[44] (PDB: 4DVY). The structured N-terminal domain (NTD) is composed of three subdomains (I−III), and the intrinsically disordered C-terminal domain (CTD) is composed from two regions, the first of which includes the phosphorylation EPIYA motifs in region IV and the C-terminus region V. (D) CagA protein fragments used in this study.

The major risk factor for gastric cancer is infection by *Helicobacter pylori* type I strains that harbor the Cag pathogenicity island (CagPAI) and express the bacterial virulence factor and oncoprotein CagA.[27,28] Not only does the presence of CagA but also polymorphisms in its sequence correlate with gastric cancer risk.[29−32] Upon infection with *H. pylori*, CagA is translocated into human gastric epithelial cells through a Type IV secretion system, a molecular syringe encoded by numerous CagPAI gene products,[33,34] assisted by an interaction with the accessory protein CagF.[35,36] CagF interacts extensively with all CagA protein domains, in which the binding determinants are mediated through a broad binding interface,[37] which is likely important for its role as a chaperone of the highly labile CagA. Once inside host cells, CagA localizes to the plasma membrane through its N-terminal region[38] and undergoes tyrosine phosphorylation at Glu-Pro-Ile-Tyr-Ala (EPIYA) motifs in its fourth, of five, domains[39,40] (Figure 1B). Translocated CagA interacts with numerous host proteins, in both phosphorylated and nonphosphorylated manners, which regulates cell growth, polarity, and motility that cause cell-morphological transformation.[38−42]

Of these myriad CagA−host protein interactions, CagA binds specifically to ASPP2 and recruits it to the plasma membrane, followed by CagA-dependent binding of ASPP2 to p53 that

DOI: 10.1021/acs.biochem.5b00084
Biochemistry 2015, 54, 3337−3347

results in proteasome-mediated p53 degradation followed by inhibition of apoptosis.[43] X-ray crystal structures of CagA show that the N-terminal region is composed of three structured domains and an intrinsically disordered C-terminal region[44,45] (Figure 1B). A crystal structure of the complex between the extreme N-terminal domain of CagA (residues 19−257) and a fragment from the ASPP2 Pro-rich domain (residues 726−782) was reported recently.[46] In this complex, 22 ASPP2 residues from the 56-residue intrinsically disordered fragment used for crystallization adopt a helical conformation and fit into a deep binding groove, maintained by flexible loops, on the CagA surface.[46] Here, we have applied numerous biochemical and biophysical methods to extensively and quantitatively examine the CagA−ASPP2 interaction further. We show that this complex is defined by multiple binding interfaces: a high affinity interaction described in the aforementioned X-ray crystal structure[46] and a novel lower-affinity interaction mediated by an intrinsically disordered region within ASPP2.

METHODS

Protein Expression and Purification. We used pRSFDuet His_6-$CagA^{1-1247}$-His_{10} and pRSFDuet His_6-$CagA^{1-885}$-His_{10} to express and purify full-length $CagA^{1-1247}$ and the N-terminal structured domains of $CagA^{1-885}$ from *H. pylori* strain 11637 as described.[37] We expressed and purified pRSET His_6-Lipoyl-TEV (HLT)-tagged $ASPP2^{693-1128}$, $ASPP2^{693-918}$, and $ASPP2^{893-1128}$ as described.[24] An additional refolding step was used to produce the final $ASPP2^{693-1128}$ protein. Briefly, purified and TEV cleaved $ASPP2^{693-1128}$ (subsequent to ion exchange purification) was concentrated and diluted 50-fold in 10 mM HEPES buffer, pH 7.4, 150 mM NaCl, and 0.05% Tween 20, including the following refolding reagents: L-arginine HCl (0.9 M), L-arginine (0.1M), cysteamine HCl (6.16 mM), and cystamine dihydrochloride (3.77 mM). The refolded protein was incubated, stirring at 4 °C for 16 h, concentrated, buffer-exchanged, and purified using a Superdex 200 column (GE Healthcare), which effectively removed the refolding reagents from the sample and ensured that the final refolded and purified protein did not exist as a mixed population of folded protein states.

A pCX full-length ASPP2 plasmid was used as a template for cloning constructs spanning ASPP2 residues 331−484, 484−692, and 331−692 into a pHLT plasmid to produce pHLT-$ASPP2^{331-484}$, pHLT-$ASPP2^{484-692}$, and pHLT-$ASPP2^{331-692}$. Soluble HLT-tagged $ASPP2^{331-484}$, $ASPP2^{484-692}$, and $ASPP2^{331-692}$ proteins were expressed in *Escherichia coli* BL21(DE3) pLysS cells (Novagen). Cells were grown in 2× YT media containing 1% glucose, at 37 °C, to an OD_{600} of 0.6−0.8. The cells were induced with 1 mM isopropyl β-D-thiogalactopyranoside (IPTG) at 21 °C for 4−8 h. Cell pellets were lysed by sonication, and HLT-tagged proteins were purified using a His Trap HP 5 mL nickel column (GE Healthcare), equilibrated with buffer (A) including 20 mM Tris, pH 7.4, 500 mM NaCl, 20 mM imidazole, 3−5 mM β-mercaptoethanol, and 10% glycerol. Proteins were eluted with buffer (B) composed of buffer (A) + 400 mM imidazole. One millimolar EDTA was added to the proteins upon elution. The eluted protein was digested overnight at 4 °C with His-tagged TEV protease and was reapplied to the Ni^{2+} His Trap column. $ASPP2^{331-692}$ and $ASPP2^{484-692}$ were further purified using cation exchange (MonoS 5/50 GL, GE Healthcare) and size exclusion (Superdex 200, GE Healthcare). $ASPP2^{331-448}$ was purified using an anion exchange (MonoQ 5/50 GL, GE Healthcare) and size exclusion chromatography (Superdex 200, GE Healthcare). Uncleaved HLT-tagged ASPP2 constructs after elution from the Ni^{2+} His Trap column were also further purified by anion exchange and size exclusion chromatography.

For expression of ^{15}N-labeled $ASPP2^{331-692}$, M9 minimal medium was used with ^{15}N-ammonium chloride. The BL21-(DE3) pLysS cells were grown at 37 °C to an OD_{600} of 0.7, induced with 1 mM IPTG, and grown 37C for 16 h. The ^{15}N-HLT-$ASPP2^{331-692}$ protein was purified as described above.

Size Exclusion Chromatography (SEC). Size exclusion chromatography of purified HLT-tagged and cleaved $ASPP2^{331-692}$ was performed on an ÄKTA Explorer (GE Healthcare) using a Superdex 200 column 10/300 GL (GE Healthcare), equilibrated with 50 mM Tris, pH 7.4, 200 mM NaCl and 1 mM EDTA. The proteins were tested in the unbound state, at concentrations of 55 μM $ASPP2^{331-692}$ and 23 μM HLT-$ASPP2^{331-692}$. The proteins eluted with a flow rate of 0.5 mL/min at 25 °C and the elution profile was recorded by continuously monitoring the UV absorbance at 280 nm. The eluted peaks of the proteins were analyzed using SDS gel and $ASPP2^{331-692}$ was analyzed for its molecular weight using mass spectrometry as well. A calibration curve was made using molecular weight standards (Bio-Rad, cat. no. 151-1901, MW 1350−670000), including bovine γ-globulin, chicken ovalbumin, and equine myoglobin.

Size Exclusion Chromatography−Multiangle Laser Light Scattering (SEC-MALS). Twenty-six micromolar (1.33 mg/mL) HLT-$ASPP2^{331-692}$ was dissolved in 10 mM potassium phosphate buffer, pH 7.4, 100 mM NaCl, 0.5 mM EDTA, and 1 mM DTT. One-hundred microliters of the protein was separated on Superdex200 Increase analytical GF column, at a flow rate of 0.75 mL/min at room temperature. A MALS miniDAWN TREOS instrument (Wyatt Technology) in line with SEC was used to measure the molecular weight of the protein.

Circular Dichroism (CD). CD spectra of 3.3 μM $ASPP2^{331-692}$ were recorded on a JASCO J-810 spectropolarimeter in 10 mM K_2HPO_4, pH 7.4, and 100 mM NaCl at 25 °C. Far-UV CD spectra were collected over a spectral range of 190−260 nm, with 0.2 nm resolution and 1.0 cm^{-1} bandwidth. Five scans were recorded, averaged, corrected for buffer contributions, and converted to molar ellipticity using CDPRO software as recommended by JASCO. Secondary structure was assessed using the DichroWeb server.[47,48] CD spectra of 4 μM HLT-tagged $ASPP2^{331-692}$ were recorded in 10 mM KH_2PO_4, pH 7.4, 100 mM NaCl, 0.5 mM EDTA, and 1 mM DTT. Changes in the CD spectra were monitored as a function of temperature from 5 to 90 °C in 5 °C steps. Data were collected each 0.1 nm, averaged over five repeats, and converted to molar ellipticity using CDPRO software as recommended by JASCO. Secondary structure was assessed using the DichroWeb server.[47,48] The molar ellipticity at 222 nm was fit to a linear model.

Nuclear Magnetic Resonance (NMR) Analysis. ^{15}N-labeled $ASPP2^{331-692}$ was dialyzed against 20 mM HEPES, pH 7.0, 100 mM NaCl, and 1 mM EDTA, concentrated to 20 μM, and 10% deuterium oxide (Sigma-Aldrich) was added to a total volume of 330 μL. All spectra were collected at 293 K on a 950 MHz Bruker Avance III NMR spectrometer, equipped with Bruker TCI cryogenic probe, in a standard $^1H-^{15}N$ transverse relaxation-optimized spectroscopy (TROSY) experiment.[49] Processing and analysis of the data were performed using Topspin 3.1 (Bruker BioSpin, Rheinstetten) and NMRView.[50]

DOI: 10.1021/acs.biochem.5b00084
Biochemistry 2015, 54, 3337−3347

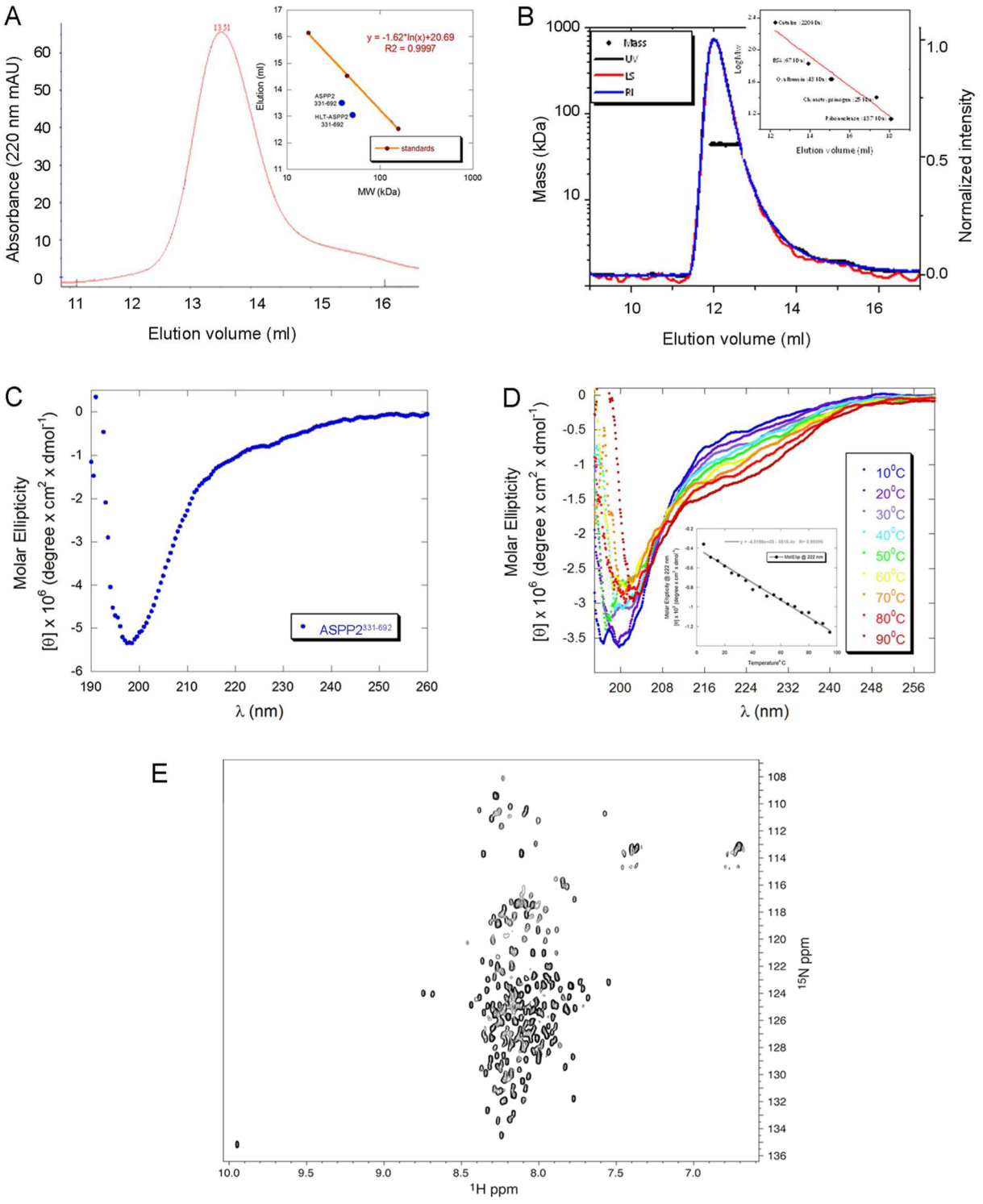

Figure 2. ASPP2 residues 331−692 are intrinsically disordered: biophysical analysis. (A) Hydrodynamic analysis. Size exclusion chromatography in 20 mM Tris, pH 7.4, 150 mM NaCl. ASPP2$^{331-692}$ eluted earlier than expected from the size exclusion chromatography column, whereas the complex of the two proteins eluted later than either of the unbound proteins. Inset: fitting the elution volume of ASPP2$^{331-692}$ to a calibration curve of higher molecular weight standards displays an apparent molecular weight of 2.2 times the calculated MW. (B) SEC-MALS analyses showing elution profile for HLT-Aspp2$^{331-692}$ on a Superdex 200 Increase column at room temperature. Absorbance profile at 280 nm and scattering at 660 nm are shown in normalized units from the measured chromatogram (right *y* axis). The mass determined from MALS analysis is shown as circles on the eluted protein (left *y* axis). (C) Far UV CD spectrum of ASPP2$^{331-692}$ in 10 mM K_2HPO_4, pH 7.4, at 25 °C, 100 mM NaCl. The CD spectrum lacked the typical signature of secondary structure. (D) Far-UV CD spectrum of HLT-ASPP2$^{331-692}$ in 10 mM KH_2PO_4, pH 7.4, 100 mM NaCl, 0.5 mM EDTA, and 1 mM DTT. Changes in the CD spectra were monitored as a function of temperature from 5 to 90 °C in 5 °C steps, presented in the linear fit of the signal at 222 nm; spectra are shown only for every 10 °C change for clarity. (E) ^{1}H−^{15}N TROSY spectrum of the ^{15}N-labeled ASPP2-A3 in 20 mM HEPES, pH 7.4, 100 mM NaCl at 20 °C showing the pattern of an unfolded protein. Most of the fingerprint resonances range over δ_{1H} 7.7−8.5 ppm, Δ = 0.8 ppm, clustered, as opposed to dispersed, as would be expected for a structured protein.

DOI: 10.1021/acs.biochem.5b00084
Biochemistry 2015, 54, 3337−3347

Disorder Predictions. The sequence of the full-length ASPP2, NCBI accession number (AC): Q13625, GI: 18652833, was submitted to eight publicly available servers implementing 16 different algorithms for protein disorder prediction. In all cases, we used the default parameters. The servers used were as follows: PONDER,[51−54] DISOPRED,[55] DisEMBL,[56] RONN,[57] IUPred,[58,59] FoldIndex,[60] and DisProt.[54,61−64] The methods are reviewed in Ferron et al.[65]

Peptide Array Screening. Peptide arrays (CelluSpots) were prepared by INTAVIS Bioanalytical Instruments AG (Köln, Germany) based on the sequences of ASPP2 and CagA (NCBI AC: ASPP2 Q13625, GI: 18652833; CagA AAF17598 GI: 6573222). The designed array included 259 15-residue partially overlapping peptides acetylated at their N-termini and attached to a cellulose membrane via their C-termini through an amide bond. The array was screened for binding His_6-$CagA^{1-1247}$-His_{10}, His_6-$CagA^{1-885}$, and HLT-$ASPP2^{693-1128}$. Protein binding and detection were performed as described for CagA.[37] We performed two controls under the same conditions as those used for the CagA−ASPP2 interactions: (i) array binding of the HLT fusion tag and (II) incubation of the anti-His-HRP antibody only with the array. In both controls, we observed no binding of the array by the antibody or the HLT fusion protein.

Surface Plasmon Resonance. SPR experiments were performed using a Biacore T100 instrument (GE Healthcare), using Biacore CM5 sensorchips (GE Healthcare). HBS-X buffer (10 mM HEPES, 150 mM NaCl, 1 mM EDTA, and 0.05% Tween 20) was used as a basic running buffer, and all experiments were performed at 10 °C. Reducing agent (5 mM β-ME or 3 mM DTT) was added when $ASPP2^{693-1128}$ or Ank-SH3 domains were used. Anti-His antibody (40 ng/μL) in 10 mM sodium acetate buffer, pH 4.0, was immobilized by standard amine coupling to all flow cells. His-tagged full-length CagA and $CagA^{1-885}$ were captured in flow cells 2−4 for 30 s. A concentration series of purified TEV-cleaved ASPP2 fragments (2−80 μM) diluted 2-fold in running buffer was injected over flow cells 1−4 for 60 s per injection (except for $ASPP2^{693-1128}$, which was injected for 120 s) and allowed to dissociate for 300s. Between binding cycles, the sensor chip surface was regenerated by washing with 10 mM glycine, pH 1.5. Affinity constants for all the proteins were calculated using a general steady-state equilibrium model with the Biacore T100 evaluation software 2.0.4.

Isothermal Titration Calorimetry. ITC experiments were performed using an iTC200 instrument (GE Healthcare). The proteins were dialyzed against 25 mM Tris, pH 7.2, or 25 mM HEPES, 150 mM sodium chloride with or without 2 mM DTT. In each experiment, the titrant concentration was 10−15-fold higher than the protein in the cell. Titrations were performed at 15−25 °C with 11−17 injections of 2 to 3 μL per injection, with at least 210 s intervals between injections. Heats of dilutions were measured and subtracted from each data set. All data were analyzed using Origin 7.0 software. Binding affinities were calculated from fitting the binding curve to a one set of sites model and averaged using two experiments (except for the $Aspp2^{693-1128}$ and $CagA^{1-885}$ reaction).

RESULTS AND DISCUSSION

While it remains unclear exactly which molecular mechanisms lead to cellular transformation in *H. pylori*-mediated gastric cancer, the ability of CagA to interact with ASPP2 and to invert its normal pro-apoptotic function is likely a contributing factor. To provide greater insight into the molecular basis of this apoptosis reprogramming mechanism, we investigated ASPP2 and quantitatively characterized its interaction with CagA by biophysical methods and mapped their interactions using peptide arrays. Employing SEC-MALS, CD, NMR analysis, sequence analysis, and disorder prediction, we identified a previously unknown intrinsically disordered region in ASPP2. Using SPR analysis, ITC, and peptide arrays, we showed that this ASPP2 intrinsically disordered region interacts specifically with CagA, thereby expanding the protein−protein interface formed in the ASPP2−CagA complex beyond that of the previously reported crystal structure.

ASPP2 Residues 331−692 Constitute an Intrinsically Disordered Region. In order to more comprehensively characterize the molecular interaction between CagA and ASPP2, we expressed and purified numerous regions of ASPP2 spanning as much of the originally identified CagA binding determinant (residues 331−831)[43] as possible (Figure 1C,D). We used several biophysical methods to assess the structural features of the ASPP2 region immediately N-terminal to the Pro-rich domain, $ASPP2^{331-692}$, which have not been analyzed previously.

Using size exclusion chromatography, we observed a low level of compactness for $ASPP2^{331-692}$, indicative of an extended conformation of this domain, typical of intrinsically disordered proteins. $ASPP2^{331-692}$ eluted as a single peak at a volume of 13.5 mL, corresponding to an apparent molecular weight of 85.1 kDa, earlier than expected for a protein of its molecular weight (38.6 kDa) according to a calibration curve of standard molecular weight markers (Figure 2A). We observed a similar elution profile for HLT-$ASPP2^{331-692}$, which includes the more structured lipoyl domain (Figure 2B), signifying that this fused domain did not alter the intrinsically disordered nature of $ASPP2^{331-692}$. HLT-$ASPP2^{331-692}$ exhibited a retention volume of 12.0 mL, corresponding to a molecular weight of 201 kDa, approximately four times larger than its calculated molecular weight (50.3 kDa). Furthermore, we determined the mass of the eluted HLT-$ASPP2^{331-692}$ peak by SEC-MALS to be 44 ± 3 kDa, similar to its calculated molecular weight, indicating that HLT-$ASPP2^{331-692}$ is a monomer, despite its elution volume being much lower than would be expected for a globular protein of this mass. Such early elution from a size exclusion column is typical of intrinsically disordered proteins and is likely due to the adoption of multiple and/or extended conformations. These SEC-MALS data suggest that HLT-$ASPP2^{331-692}$ is an intrinsically disordered protein that exists in solution in a monomeric state.

We also analyzed $ASPP2^{331-692}$ by far-UV CD and observed a spectrum that consisted mainly of a minimum at 200 nm, indicative of a high content of unstructured protein (Figure 2C). We calculated the secondary structure content[47,48] of $ASPP2^{331-692}$ to be 56% disordered, 2% helix, 28% strand, and 14% turn conformations. To analyze the effect of temperature on the disordered conformation of this segment, we monitored the changes of the CD signal of HLT-$ASPP2^{331-692}$ at 222 nm as a function of temperature from 5 to 90 °C, in 5 °C steps (Figure 2D). The spectra exhibited a linear increase of ellipticity with increasing temperature (Figure 2D, inset), indicating an apparent temperature-induced formation of residual secondary structure. We found these conformational changes to be reversible (data not shown).

DOI: 10.1021/acs.biochem.5b00084
Biochemistry 2015, 54, 3337−3347

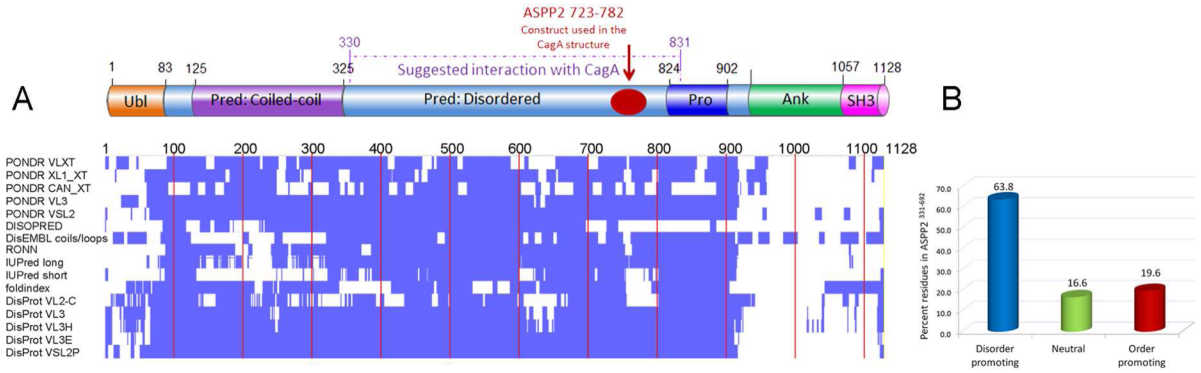

Figure 3. ASPP2 residues 331−692 are intrinsically disordered: bioinformatic analysis. (A) Sequence analysis of the order- and disorder-promoting residues in the sequence of ASPP2$^{331-692}$. The residues are classified as order-promoting (I, L, V, W, F, Y, and C), disorder-promoting (E, K, R, G, Q, S, P, and A), and neutral (all others). (B) Disorder predictions for the ASPP2 sequence were performed using 16 algorithms in publicly available servers presented in each row. Regions predicted to be disordered are represented in purple.

Finally, we analyzed ASPP2$^{331-692}$ by NMR spectroscopy. The HSQC-TROSY spectrum of ^{15}N-labeled ASPP2$^{331-692}$ exhibited a pattern typical for disordered proteins (Figure 2E), in which the observed resonances of the amide protons are dispersed in a narrow cluster ranged from δ_{1H} 7.7 to 8.5 ppm (Δ = 0.8 ppm), unlike wider distributions typical for structured proteins.[66,67] We observed only one set of resonances in the NMR spectrum, indicating that ASPP2$^{331-692}$ exists in a monomeric state at the high concentrations used for NMR.

Next, we performed a statistical analysis of ASPP2 (Figure 3A) indicating that 63.8% of this region is composed of disorder promoting residues (E, K, R, G, Q, S, P, and A), compared to 19.6% order-promoting (I, L, V, W, F, Y, and C) and 16.6% neutral residues.[52,68,69] Upon submitting the sequence of full-length ASPP2 to eight publicly available bioinformatics servers employing 16 different algorithms for protein disorder prediction, we observed that the N-terminal (residues 1−80) and C-terminal regions (residues 920−1128) were predicted to be effectively ordered, whereas the majority of the remainder of the protein, including ASPP2$^{331-692}$, was predicted to be disordered (Figure 3B). These predictions are in agreement with other structural properties previously reported by us and others, including the structured N-terminal and Ank-SH3 domains[7,23] and the intrinsically disordered nature of the Pro-rich domain.[24]

CagA Interacts with ASPP2$^{331-692}$ through a Binding Determinant Spanning Residues 484−692. The interaction between CagA and ASPP2 was previously shown to involve a region of ASPP2 spanning residues 331−831.[43] Thus, we sought to determine if the intrinsically disordered ASPP2$^{331-692}$ region contributed to the CagA−ASPP2 interaction. We quantitatively characterized the interaction of ASPP2$^{331-692}$ with CagA by SPR and observed that ASPP2$^{331-692}$ bound full-length CagA with a dissociation constant (K_D) of 15 μM (Figure 4A). By further dissecting ASPP2$^{331-692}$ into two nonoverlapping parts, we observed that this interaction is mediated solely through residues 484−692, as ASPP2$^{484-692}$ bound CagA with a K_D of 13 μM (Figure 4B), with no contribution to binding from the N-terminal part, ASPP2$^{331-484}$ (Figure 4C). Both ASPP2$^{331-692}$ and ASPP2$^{484-692}$ interacted with the first three domains of CagA alone, CagA$^{1-885}$, with similar binding affinities (K_D's of 4 and 5 μM, respectively) as they did to full-length CagA (Figure 4D,E). These results indicate that ASPP2 residues 484−692, within the newly identified intrinsically disordered region, bind to CagA residues 1−885, which comprise its first three structured domains. All of the ASPP2$^{331-692}$−CagA binding affinities that we determined by SPR are summarized in Table 1.

CagA Interacts with Peptides Derived Predominantly from ASPP2$^{484-692}$. To more precisely map the binding determinants within the intrinsically disordered ASPP2$^{331-692}$ region that mediate interaction with CagA, we employed a peptide array screening approach.[70] We screened an array of 41 partially overlapping peptides derived from ASPP2$^{331-692}$ for binding to CagA$^{1-885}$ (Supporting Information Table S1). Although CagA$^{1-885}$ bound several peptides (I24-ASPP2$^{386-400}$, J1-ASPP2$^{397-411}$, and J6-ASPP2$^{440-454}$) within the ASPP2$^{331-484}$ region that did not bind as a contiguous protein fragment in our SPR experiments, peptides derived from the ASPP2$^{484-692}$ region that confers CagA binding were both more numerous and prominent (Figure 4F). In particular, peptides centered within a set of binding peptides (J12-ASPP2$^{494-508}$ and J17-ASPP2$^{541-555}$) and peptides of the highest intensity (J21-ASPP2$^{577-591}$ and K6-ASPP2$^{656-670}$) are likely to comprise the noncontiguous binding determinants of the ASPP2$^{484-692}$ protein fragment.

ASPP2$^{484-692}$ Interacts with the N-Terminal Domain of CagA. To determine if the intrinsically disordered ASPP2$^{484-692}$ region bound to the N-terminal domain of CagA, as does the ASPP2$^{746-765}$ peptide fragment observed in the ASPP2−CagA crystal structure,[46] we measured the interaction of ASPP2$^{484-692}$ with both CagA$^{1-885}$ (inclusive of the N-terminal domain) and CagA$^{256-885}$ (missing the N-terminal domain) by ITC. When we measured the thermodynamic parameters of binding between ASPP2$^{484-692}$ and CagA$^{1-885}$ (Figure 4G and Table 1), we observed binding with similar affinity (K_D = 4.9 ± 0.5 μM) to that from the analogous experiment carried out by SPR. Conversely, we observed no binding between ASPP2$^{484-692}$ and CagA$^{256-885}$ by both ITC (Figure 4H and Table 1) and SPR (Figure 4I). These data indicate that ASPP2$^{484-692}$ interacts with the extreme N-terminal domain of CagA, inclusive of residues 1−256, which also contains the binding site for ASPP2$^{746-765}$.

Thermodynamic Analysis of CagA Interactions with the ASPP2 Pro-Rich and Ank-SH3 Regions. The CagA fragment spanning residues 1−877 interacts *in vivo* with an ASPP2 fragment inclusive of residues 330−831 but not with ASPP2 fragments restricted to either residues 1−330 or 920−1128.[43] This binding region, ASPP2$^{330-831}$, extends through the

DOI: 10.1021/acs.biochem.5b00084
Biochemistry 2015, 54, 3337−3347

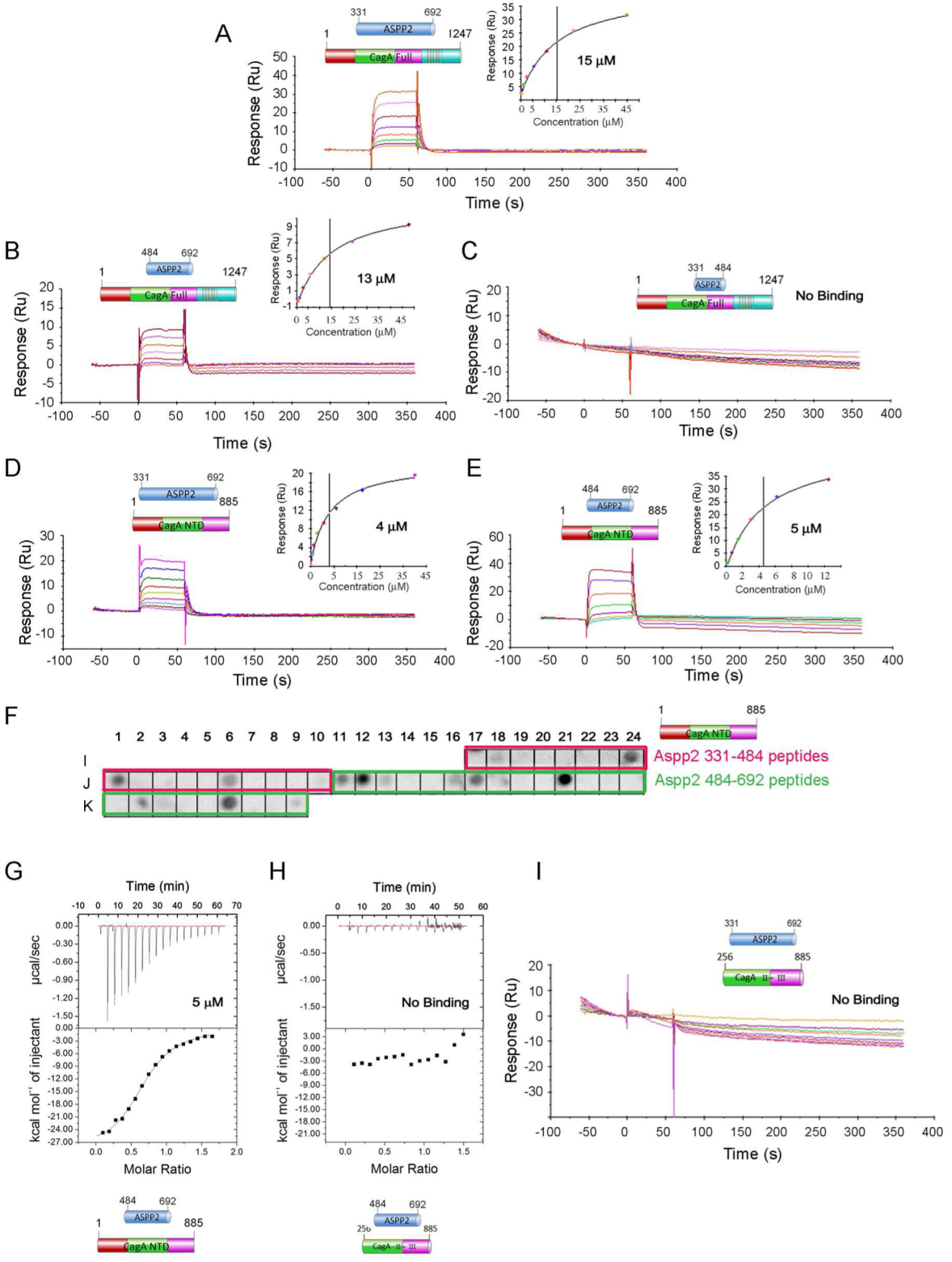

Figure 4. Dissecting the interaction between CagA and ASPP2$^{331-692}$ fragments. (A–E) Surface plasmon resonance (SPR) analysis of the interaction between a ASPP2 constructs and $(His)_6$-CagA$^{1-1248}$-$(His)_{10}$ and $(His)_6$-CagA$^{1-885}$ captured by an anti-His antibody immobilized chip. The affinity deduced from the steady-state analysis is presented in the inset of every binding curve. (F) Representative peptide array results showing the binding of $(His)_6$-CagA$^{1-885}$ to Aspp2$^{331-692}$-derived peptides on the array, as detected using HRP-conjugated anti-His antibody. (G–H) Isothermal titration calorimetry (ITC) binding analysis of ASPP2$^{484-692}$ to CagA$^{1-885}$ and CagA$^{256-885}$. (I) SPR binding analysis of ASPP2$^{484-692}$ to CagA$^{256-885}$.

intrinsically disordered region described above and into the ASPP2 Pro-rich domain. More specifically, ASPP2 residues 746–765, part of the ASPP2 Pro-rich region, form an α-helix that binds in a groove on the surface of the N-terminal structured domain of CagA.[46] To quantify and analyze the thermodynamic profile of the CagA interactions with the Pro-

DOI: 10.1021/acs.biochem.5b00084
Biochemistry 2015, 54, 3337–3347

Table 1. Binding Affinities of ASPP2 Fragments with CagA

ASPP2 domain	CagA domain	K_D (μM)	error (μM)	N	ΔH (kcal/mol)	ΔS (cal/K/mol)	$T\Delta S$ (kcal/mol)	ΔG (kcal/mol)
Surface Plasmon Resonance Analysis[b]								
331−692	full length	15.2	0.2					
484−692	full length	13	1.5					
331−484	full length	NB[a]						
331−692	1−885	4.2	0.2					
484−692	1−885	4.9	0.5					
Isothermal Titration Calorimetry Analysis[c]								
484−692	1−885	4.9	0.5	0.65	−30.71	−78.65	−23.20	−7.50
484−692	256−885	NB						
693−1128	1−885	0.062		0.93	−14.9	−18.6	−5.36	−9.54
893−1128	full length	NB						
693−918	1−885	0.027	0.001	0.925	−12.9	−8.82	−2.54	−10.4

[a]NB, no binding. [b]SPR affinities were calculated by steady-state equilibrium model and averaged using two experiments. [c]ITC affinities were calculated from fitting the binding curve to a one set of sites model and averaged using two experiments (except for the Aspp2$^{693-1128}$ and CagA$^{1-885}$ reaction). ITC deduced thermodynamic parameters of the relevant interactions are presented.

rich and Ank-SH3 domains of ASPP2, we performed isothermal titration calorimetry using CagA$^{1-885}$ and the ASPP2 Pro-rich and Ank-SH3 domains either alone (ASPP2$^{693-918}$ and ASPP2$^{893-1128}$, respectively) or together (as a single fused fragment, ASPP2$^{693-1128}$). We found that CagA$^{1-885}$ bound ASPP2$^{693-1128}$, inclusive of both Pro-rich and Ank-SH3 domains, as a 1:1 complex with an affinity of 62 nM (Figure 5A). This interaction is entirely dependent on the presence of the Pro-rich domain, as we detected no binding between CagA and the ASPP2 Ank-SH3 domain (Figure 5B). The thermodynamic parameters of these ITC experiments are summarized in Table 1.

Mapping CagA Interactions with the ASPP2 Pro-Rich and Ank-SH3 Regions. We screened an array containing 44 partially overlapping peptides covering the entire ASPP2 Pro-rich and Ank-SH3 domains for binding to CagA$^{1-885}$ (Supporting Information Table S1). CagA$^{1-885}$ bound peptides derived from both ASPP2 domains (Figure 5C). However, many of the peptides from the Pro-rich domain that exhibited binding occurred in pairs or triplets (i.e., overlapping and contiguous with one another), whereas all of the binding peptides from the Ank-SH3 domain occurred as single peptides surrounded by nonbinding peptides. In the ASPP2 Pro-rich domain, three sets of binding peptides included (i) K12-ASPP2$^{710-724}$/K13-ASPP2$^{721-735}$, (ii) K15-ASPP2$^{739-753}$/K16-ASPP2$^{746-760}$, and (iii) L8-ASPP2$^{890-904}$/L9-ASPP2$^{901-915}$/L10-ASPP2$^{908-922}$. The first peptide set includes ASPP2 residues 710−735 that are N-terminal to the construct used for crystallization but included in the fragment, residues 684−891, found to bind CagA by yeast two-hybrid analysis.[46] The second peptide set includes ASPP2 residues 739−760 that form the majority of the α-helix, residues 746−765, observed to bind to CagA in the crystal structure.[46] The third peptide set includes ASPP2 residues 890−922 that reside directly C-terminal to the yeast two-hybrid binding fragment.[46] These data confirm that our peptide array assays can detect the known CagA binding determinant of ASPP2, the α-helix formed by residues 746−765, and suggest that other regions of the ASPP2 Pro-rich domain contribute to CagA binding.

ASPP2$^{693-918}$ Interacts with the N-Terminal Domain of CagA. To determine whether any of these potential interactions between the ASPP2 Pro-rich domain and CagA involve CagA domains other its N-terminal domain, we performed ITC analysis of ASPP2$^{693-918}$ binding with both CagA$^{1-885}$ (containing the first three structured domains of CagA). We observed ASPP2$^{693-918}$ binding to CagA$^{1-885}$ with a similar affinity, K_D = 27 nM (Figure 5D), as that for the ASPP2$^{693-1128}$ fragment inclusive of the Pro-rich and Ank-SH3 domains. Notably, the longer ASPP2 fragment had a substantially higher entropic barrier to binding CagA$^{1-885}$, ΔS = −18.6 cal/K/mol, than did the ASPP2 Pro-rich domain alone, ΔS = −8.8 cal/K/mol (Table 1), potentially indicating an increase in the overall conformational ordering of the Ank-SH3 domain upon binding to the Pro-rich domain.

Physiological Implications of the Extended ASPP2−CagA Binding Interface. We have previously shown that ASPP2$^{693-918}$ is intrinsically disordered and is involved in ASPP2 intramolecular interactions between the Pro-rich and Ank-SH3 domains that regulate various ASPP2 interactions with other proteins.[24] Together, ASPP2$^{331-692}$ and ASPP2$^{693-918}$ comprise a vast intrinsically disordered region, connecting the structured termini of ASPP2 that mediate numerous interactions important for ASPP2 functions.[8] That CagA evolved to interact with the intrinsically disordered regions of ASPP2 that mediate fewer (i.e., two) known interactions, and not the structured termini that mediate many known interactions, may be important for its function to inhibit transformed host cells from proceeding with their intended apoptotic program. This mode of interaction could enable ASPP2 to interact with p53, via its Ank-SH3 domain, without competing for CagA binding. Additionally, since both binding regions of ASPP2 interact with the N-terminal Domain I of CagA, the induction of a novel loop or short stretch of secondary structure that minimally encompasses ASPP2 residues 693−746 is possible. If this region of ASPP2 were structurally distinct between its intrinsically disordered unbound state and its CagA-bound form, then it could provide a unique molecular surface for the recruitment of proteins that promote the degradation of p53. This is just one of many potential molecular mechanisms by which CagA might subvert the normal function of ASPP2 that is suggested by our biochemical and biophysical analyses of this protein−protein interaction. Additional aspects of the molecular mechanisms by which CagA, through its binding to ASPP2, inverts the p53 tumor suppressor pathway of the host, however, remain to be elucidated.

DOI: 10.1021/acs.biochem.5b00084
Biochemistry 2015, 54, 3337−3347

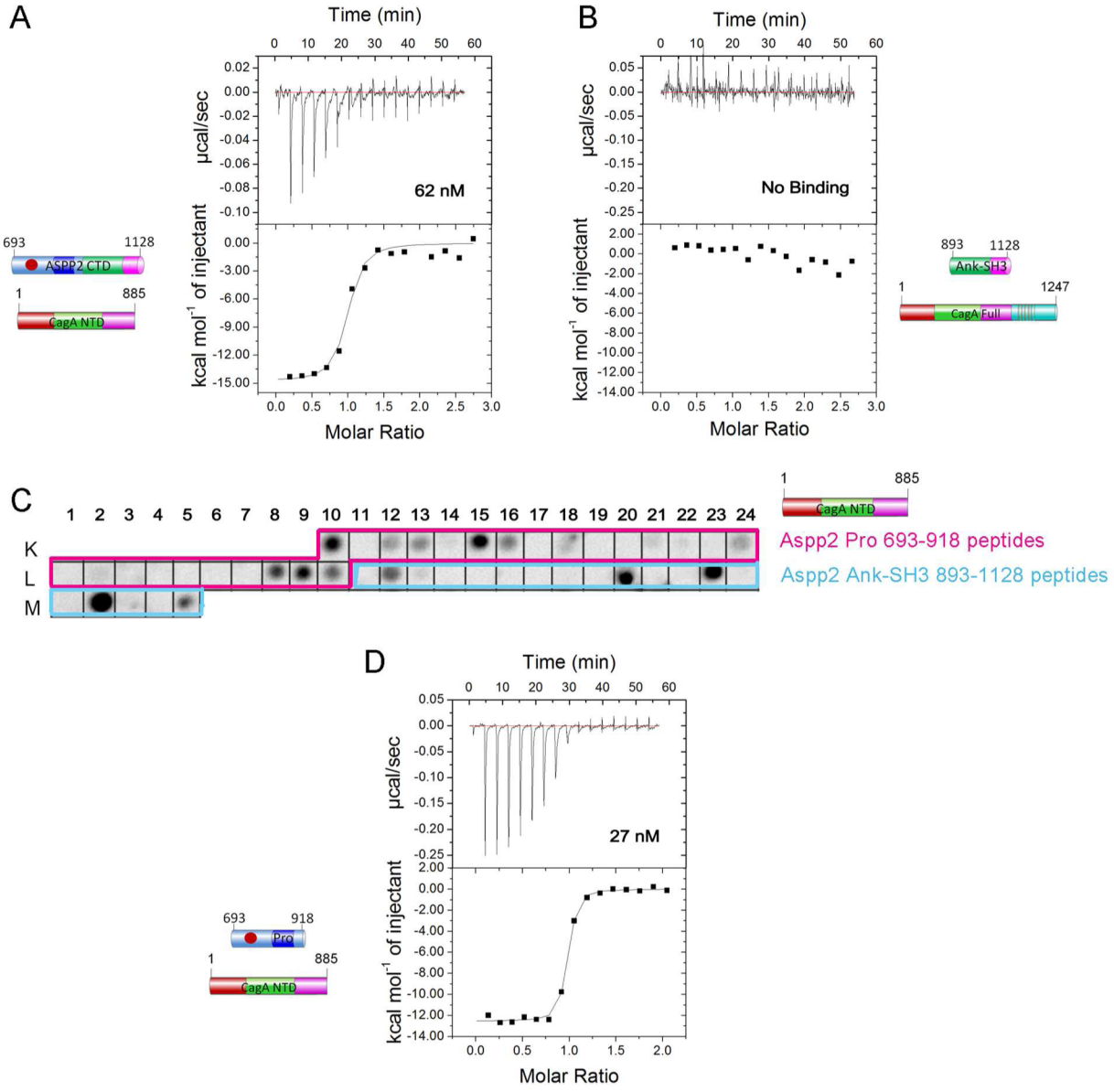

Figure 5. Dissecting the interaction between CagA and ASPP2-CTD$^{693-1128}$ fragments. (A, B) Isothermal titration calorimetry (ITC) binding analysis of CagA$^{1-885}$ to ASPP2-CTD$^{693-1128}$ and ASPP2-Pro$^{693-819}$. (C) Representative peptide array results showing the binding of $(His)_6$-CagA$^{1-885}$ to ASPP2$^{693-1128}$-derived peptides on the array. (D) Isothermal titration calorimetry (ITC) binding analysis of ASPP2$^{693-1128}$ to CagA$^{1-885}$.

■ ASSOCIATED CONTENT

Supporting Information

Data related to the peptide array analysis of ASPP2-derived peptides interacting with CagA$^{1-885}$. The Supporting Information is available free of charge online at The Supporting Information is available free of charge on the ACS Publications website at DOI: 10.1021/acs.biochem.5b00084.

■ AUTHOR INFORMATION

Corresponding Author

*Tel.: 410-706-7468; Fax: 410-706-6695; E-mail: esundberg@ihv.umaryland.edu.

Present Address

⊥(T.H.R.) University of Haifa, Department of Human Biology, Mount Carmel, Haifa 3498838, Israel.

Funding

This work was supported, in part, by an Alexander von Humboldt Foundation Experienced Researcher Fellowship to E.J.S. as well as a Fulbright Scholarship and ISEF Fellowship to T.H.R. A.F. is supported by grants from the Israel Cancer Association, Israel Science Foundation (ISF) and the Israel Cancer Research Foundation (ICRF) and by the Minerva Center for Bio-Hybrid Complex Systems. A.I. and H.A. are supported by the Dalia and Dan Meydan Fellowship for advanced degree students at the Hebrew University of Jerusalem.

Notes

The authors declare no competing financial interest.

■ ACKNOWLEDGMENTS

We thank Dr. Kristen Varney at the NMR Center of the University of Maryland School of Medicine for her help with

DOI: 10.1021/acs.biochem.5b00084
Biochemistry 2015, 54, 3337−3347

collecting NMR spectra, as well as Dr. Jace Jones at the mass spectrometry facility of the University of Maryland School of Pharmacy.

REFERENCES

(1) Thompson, C. B. (1995) Apoptosis in the pathogenesis and treatment of disease. *Science 267*, 1456−1462.
(2) Evan, G. I., and Vousden, K. H. (2001) Proliferation, cell cycle and apoptosis in cancer. *Nature 411*, 342−348.
(3) Brown, J. M., and Attardi, L. D. (2005) The role of apoptosis in cancer development and treatment response. *Nat. Rev. Cancer 5*, 231−237.
(4) Fesik, S. W. (2005) Promoting apoptosis as a strategy for cancer drug discovery. *Nat. Rev. Cancer 5*, 876−885.
(5) Reed, J. C. (2006) Drug insight: cancer therapy strategies based on restoration of endogenous cell death mechanisms. *Nat. Clin. Pract. Oncol. 3*, 388−398.
(6) Samuels-Lev, Y., O'Connor, D. J., Bergamaschi, D., Trigiante, G., Hsieh, J. K., Zhong, S., Campargue, I., Naumovski, L., Crook, T., and Lu, X. (2001) ASPP proteins specifically stimulate the apoptotic function of p53. *Mol. Cell 8*, 781−794.
(7) Gorina, S., and Pavletich, N. P. (1996) Structure of the p53 tumor suppressor bound to the ankyrin and SH3 domains of 53BP2. *Science 274*, 1001−1005.
(8) Iosub-Amir, A., and Friedler, A. (2014) Protein−protein interactions of ASPP2: an emerging therapeutic target. *Med. Chem. Commun. 5*, 1435−1443.
(9) Liu, Z. J., Lu, X., Zhang, Y., Zhong, S., Gu, S. Z., Zhang, X. B., Yang, X., and Xin, H. M. (2005) Downregulated mRNA expression of ASPP and the hypermethylation of the 5′-untranslated region in cancer cell lines retaining wild-type p53. *FEBS Lett. 579*, 1587−1590.
(10) Takahashi, N., Kobayashi, S., Jiang, X., Kitagori, K., Imai, K., Hibi, Y., and Okamoto, T. (2004) Expression of 53BP2 and ASPP2 proteins from TP53BP2 gene by alternative splicing. *Biochem. Biophys. Res. Commun. 315*, 434−438.
(11) Yang, J. P., Hori, M., Takahashi, N., Kawabe, T., Kato, H., and Okamoto, T. (1999) NF-kappaB subunit p65 binds to 53BP2 and inhibits cell death induced by 53BP2. *Oncogene 18*, 5177−5186.
(12) Kobayashi, S., Kajino, S., Takahashi, N., Kanazawa, S., Imai, K., Hibi, Y., Ohara, H., Itoh, M., and Okamoto, T. (2005) 53BP2 induces apoptosis through the mitochondrial death pathway. *Genes Cells 10*, 253−260.
(13) Schittenhelm, M. M., Illing, B., Ahmut, F., Rasp, K. H., Blumenstock, G., Dohner, K., Lopez, C. D., and Kampa-Schittenhelm, K. M. (2013) Attenuated expression of apoptosis stimulating protein of p53-2 (ASPP2) in human acute leukemia is associated with therapy failure. *PLoS One 8*, e80193.
(14) Robinson, R. A., Lu, X., Jones, E. Y., and Siebold, C. (2008) Biochemical and structural studies of ASPP proteins reveal differential binding to p53, p63, and p73. *Structure 16*, 259−268.
(15) Bergamaschi, D., Samuels, Y., Jin, B., Duraisingham, S., Crook, T., and Lu, X. (2004) ASPP1 and ASPP2: common activators of p53 family members. *Mol. Cell. Biol. 24*, 1341−1350.
(16) Naumovski, L., and Cleary, M. L. (1996) The p53-binding protein 53BP2 also interacts with Bc12 and impedes cell cycle progression at G2/M. *Mol. Cell. Biol. 16*, 3884−3892.
(17) Katz, C., Benyamini, H., Rotem, S., Lebendiker, M., Danieli, T., Iosub, A., Refaely, H., Dines, M., Bronner, V., Bravman, T., Shalev, D. E., Rudiger, S., and Friedler, A. (2008) Molecular basis of the interaction between the antiapoptotic Bcl-2 family proteins and the proapoptotic protein ASPP2. *Proc. Natl. Acad. Sci. U.S.A. 105*, 12277−12282.
(18) Helps, N. R., Barker, H. M., Elledge, S. J., and Cohen, P. T. (1995) Protein phosphatase 1 interacts with p53BP2, a protein which binds to the tumour suppressor p53. *FEBS Lett. 377*, 295−300.
(19) Cao, Y., Hamada, T., Matsui, T., Date, T., and Iwabuchi, K. (2004) Hepatitis C virus core protein interacts with p53-binding protein, 53BP2/Bbp/ASPP2, and inhibits p53-mediated apoptosis. *Biochem. Biophys. Res. Commun. 315*, 788−795.
(20) Wang, Z. P., Liu, Y. G., Takahashi, M., Van Hook, K., Kampa-Schittenhelm, K. M., Sheppard, B. C., Sears, R. C., Stork, P. J. S., and Lopez, C. D. (2013) N terminus of ASPP2 binds to Ras and enhances Ras/Raf/MEK/ERK activation to promote oncogene-induced senescence. *Proc. Natl. Acad. Sci. U.S.A. 110*, 312−317.
(21) Wang, X. D., Lapi, E., Sullivan, A., Ratnayaka, I., Goldin, R., Hay, R., and Lu, X. (2011) SUMO-modified nuclear cyclin D1 bypasses Ras-induced senescence. *Cell Death Differ. 18*, 304−314.
(22) Cong, W., Hirose, T., Harita, Y., Yamashita, A., Mizuno, K., Hirano, H., and Ohno, S. (2010) ASPP2 regulates epithelial cell polarity through the PAR complex. *Curr. Biol. 20*, 1408−1414.
(23) Tidow, H., Andreeva, A., Rutherford, T. J., and Fersht, A. R. (2007) Solution structure of ASPP2 N-terminal domain (N-ASPP2) reveals a ubiquitin-like fold. *J. Mol. Biol. 371*, 948−958.
(24) Rotem, S., Katz, C., Benyamini, H., Lebendiker, M., Veprintsev, D., Rudiger, S., Danieli, T., and Friedler, A. (2008) The structure and interactions of the proline-rich domain of ASPP2. *J. Biol. Chem. 283*, 18990−18999.
(25) Rotem-Bamberger, S., Katz, C., and Friedler, A. (2013) Regulation of ASPP2 interaction with p53 core domain by an intramolecular autoinhibitory mechanism. *PLoS One 8*, e58470.
(26) Godin-Heymann, N., Wang, Y., Slee, E., and Lu, X. (2013) Phosphorylation of ASPP2 by RAS/MAPK pathway is critical for its full pro-apoptotic function. *PLoS One 8*, e82022.
(27) Censini, S., Lange, C., Xiang, Z., Crabtree, J. E., Ghiara, P., Borodovsky, M., Rappuoli, R., and Covacci, A. (1996) cag, a pathogenicity island of *Helicobacter pylori*, encodes type I-specific and disease-associated virulence factors. *Proc. Natl. Acad. Sci. U.S.A. 93*, 14648−14653.
(28) Kusters, J. G., van Vliet, A. H., and Kuipers, E. J. (2006) Pathogenesis of *Helicobacter pylori* infection. *Clin. Microbiol. Rev. 19*, 449−490.
(29) Parsonnet, J., Friedman, G. D., Orentreich, N., and Vogelman, H. (1997) Risk for gastric cancer in people with CagA positive or CagA negative *Helicobacter pylori* infection. *Gut 40*, 297−301.
(30) Franco, A. T., Johnston, E., Krishna, U., Yamaoka, Y., Israel, D. A., Nagy, T. A., Wroblewski, L. E., Piazuelo, M. B., Correa, P., and Peek, R. M., Jr. (2008) Regulation of gastric carcinogenesis by *Helicobacter pylori* virulence factors. *Cancer Res. 68*, 379−387.
(31) Blaser, M. J., Perez-Perez, G. I., Kleanthous, H., Cover, T. L., Peek, R. M., Chyou, P. H., Stemmermann, G. N., and Nomura, A. (1995) Infection with *Helicobacter pylori* strains possessing cagA is associated with an increased risk of developing adenocarcinoma of the stomach. *Cancer Res. 55*, 2111−2115.
(32) Israel, D. A., Salama, N., Arnold, C. N., Moss, S. F., Ando, T., Wirth, H. P., Tham, K. T., Camorlinga, M., Blaser, M. J., Falkow, S., and Peek, R. M., Jr. (2001) *Helicobacter pylori* strain-specific differences in genetic content, identified by microarray, influence host inflammatory responses. *J. Clin. Invest. 107*, 611−620.
(33) Alvarez-Martinez, C. E., and Christie, P. J. (2009) Biological diversity of prokaryotic type IV secretion systems. *Microbiol. Mol. Biol. Rev. 73*, 775−808.
(34) Voth, D. E., Broederdorf, L. J., and Graham, J. G. (2012) Bacterial Type IV secretion systems: versatile virulence machines. *Future Microbiol. 7*, 241−257.
(35) Couturier, M. R., Tasca, E., Montecucco, C., and Stein, M. (2006) Interaction with CagF is required for translocation of CagA into the host via the Helicobacter pylori type IV secretion system. *Infect. Immun. 74*, 273−281.
(36) Pattis, I., Weiss, E., Laugks, R., Haas, R., and Fischer, W. (2007) The *Helicobacter pylori* CagF protein is a type IV secretion chaperone-like molecule that binds close to the C-terminal secretion signal of the CagA effector protein. *Microbiology 153*, 2896−2909.
(37) Bonsor, D. A., Weiss, E., Iosub-Amir, A., Reingewertz, T. H., Chen, T. W., Haas, R., Friedler, A., Fischer, W., and Sundberg, E. J. (2013) Characterization of the translocation-competent complex

DOI: 10.1021/acs.biochem.5b00084
Biochemistry 2015, 54, 3337−3347

between the *Helicobacter pylori* oncogenic protein CagA and the accessory protein CagF. *J. Biol. Chem. 288*, 32897−32909.
(38) Bagnoli, F., Buti, L., Tompkins, L., Covacci, A., and Amieva, M. R. (2005) *Helicobacter pylori* CagA induces a transition from polarized to invasive phenotypes in MDCK cells. *Proc. Natl. Acad. Sci. U.S.A. 102*, 16339−16344.
(39) Stein, M., Bagnoli, F., Halenbeck, R., Rappuoli, R., Fantl, W. J., and Covacci, A. (2002) c-Src/Lyn kinases activate *Helicobacter pylori* CagA through tyrosine phosphorylation of the EPIYA motifs. *Mol. Microbiol. 43*, 971−980.
(40) Poppe, M., Feller, S. M., Romer, G., and Wessler, S. (2007) Phosphorylation of *Helicobacter pylori* CagA by c-Abl leads to cell motility. *Oncogene 26*, 3462−3472.
(41) Amieva, M. R., Vogelmann, R., Covacci, A., Tompkins, L. S., Nelson, W. J., and Falkow, S. (2003) Disruption of the epithelial apical-junctional complex by *Helicobacter pylori* CagA. *Science 300*, 1430−1434.
(42) Murata-Kamiya, N., Kurashima, Y., Teishikata, Y., Yamahashi, Y., Saito, Y., Higashi, H., Aburatani, H., Akiyama, T., Peek, R. M., Jr., Azuma, T., and Hatakeyama, M. (2007) *Helicobacter pylori* CagA interacts with E-cadherin and deregulates the beta-catenin signal that promotes intestinal transdifferentiation in gastric epithelial cells. *Oncogene 26*, 4617−4626.
(43) Buti, L., Spooner, E., Van der Veen, A. G., Rappuoli, R., Covacci, A., and Ploegh, H. L. (2011) *Helicobacter pylori* cytotoxin-associated gene A (CagA) subverts the apoptosis-stimulating protein of p53 (ASPP2) tumor suppressor pathway of the host. *Proc. Natl. Acad. Sci. U.S.A. 108*, 9238−9243.
(44) Hayashi, T., Senda, M., Morohashi, H., Higashi, H., Horio, M., Kashiba, Y., Nagase, L., Sasaya, D., Shimizu, T., Venugopalan, N., Kumeta, H., Noda, N. N., Inagaki, F., Senda, T., and Hatakeyama, M. (2012) Tertiary structure−function analysis reveals the pathogenic signaling potentiation mechanism of *Helicobacter pylori* oncogenic effector CagA. *Cell Host Microbe 12*, 20−33.
(45) Kaplan-Turkoz, B., Jimenez-Soto, L. F., Dian, C., Ertl, C., Remaut, H., Louche, A., Tosi, T., Haas, R., and Terradot, L. (2012) Structural insights into *Helicobacter pylori* oncoprotein CagA interaction with beta1 integrin. *Proc. Natl. Acad. Sci. U.S.A. 109*, 14640−14645.
(46) Nesic, D., Buti, L., Lu, X., and Stebbins, C. E. (2014) Structure of the *Helicobacter pylori* CagA oncoprotein bound to the human tumor suppressor ASPP2. *Proc. Natl. Acad. Sci. U.S.A. 111*, 1562−1567.
(47) Whitmore, L., and Wallace, B. A. (2004) DICHROWEB, an online server for protein secondary structure analyses from circular dichroism spectroscopic data. *Nucleic Acids Res. 32*, W668−W673.
(48) Whitmore, L., and Wallace, B. A. (2008) Protein secondary structure analyses from circular dichroism spectroscopy: methods and reference databases. *Biopolymers 89*, 392−400.
(49) Salzmann, M., Pervushin, K., Wider, G., Senn, H., and Wuthrich, K. (1998) TROSY in triple-resonance experiments: new perspectives for sequential NMR assignment of large proteins. *Proc. Natl. Acad. Sci. U.S.A. 95*, 13585−13590.
(50) Johnson, B. A. (2004) Using NMRView to visualize and analyze the NMR spectra of macromolecules. *Methods Mol. Biol. 278*, 313−352.
(51) Andersen, P. S., Lavoie, P. M., Sekaly, R. P., Churchill, H., Kranz, D. M., Schlievert, P. M., Karjalainen, K., and Mariuzza, R. A. (1999) Role of the T cell receptor alpha chain in stabilizing TCR-superantigen- MHC class II complexes. *Immunity 10*, 473−483.
(52) Romero, P., Obradovic, Z., Li, X., Garner, E. C., Brown, C. J., and Dunker, A. K. (2001) Sequence complexity of disordered protein. *Proteins 42*, 38−48.
(53) Romero, O., and Dunker, K. (1997) Sequence data analysis for long disordered regions prediction in the calcineurin family. *Genome Inf. Ser. 8*, 110−124.
(54) Obradovic, Z., Peng, K., Vucetic, S., Radivojac, P., and Dunker, A. K. (2005) Exploiting heterogeneous sequence properties improves prediction of protein disorder. *Proteins 61*, 176−182.
(55) Buchan, D. W., Minneci, F., Nugent, T. C., Bryson, K., Jones, D. T. Scalable web services for the PSIPRED protein analysis workbench, *Nucleic Acids Res. 41*, W349−357.
(56) Linding, R., Jensen, L. J., Diella, F., Bork, P., Gibson, T. J., and Russell, R. B. (2003) Protein disorder prediction: implications for structural proteomics. *Structure 11*, 1453−1459.
(57) Yang, Z. R., Thomson, R., McNeil, P., and Esnouf, R. M. (2005) RONN: the bio-basis function neural network technique applied to the detection of natively disordered regions in proteins. *Bioinformatics 21*, 3369−3376.
(58) Dosztanyi, Z., Csizmok, V., Tompa, P., and Simon, I. (2005) The pairwise energy content estimated from amino acid composition discriminates between folded and intrinsically unstructured proteins. *J. Mol. Biol. 347*, 827−839.
(59) Dosztanyi, Z., Csizmok, V., Tompa, P., and Simon, I. (2005) IUPred: web server for the prediction of intrinsically unstructured regions of proteins based on estimated energy content. *Bioinformatics 21*, 3433−3434.
(60) Prilusky, J., Felder, C. E., Zeev-Ben-Mordehai, T., Rydberg, E. H., Man, O., Beckmann, J. S., Silman, I., and Sussman, J. L. (2005) FoldIndex: a simple tool to predict whether a given protein sequence is intrinsically unfolded. *Bioinformatics 21*, 3435−3438.
(61) Vucetic, S., Brown, C. J., Dunker, A. K., and Obradovic, Z. (2003) Flavors of protein disorder. *Proteins 52*, 573−584.
(62) Obradovic, Z., Peng, K., Vucetic, S., Radivojac, P., Brown, C. J., and Dunker, A. K. (2003) Predicting intrinsic disorder from amino acid sequence. *Proteins 53*, 566−572.
(63) Peng, K., Vucetic, S., Radivojac, P., Brown, C. J., Dunker, A. K., and Obradovic, Z. (2005) Optimizing long intrinsic disorder predictors with protein evolutionary information. *J. Bioinf. Comput. Biol. 3*, 35−60.
(64) Peng, K., Radivojac, P., Vucetic, S., Dunker, A. K., and Obradovic, Z. (2006) Length-dependent prediction of protein intrinsic disorder. *BMC Bioinf. 7*, 208.
(65) Ferron, F., Longhi, S., Canard, B., and Karlin, D. (2006) A practical overview of protein disorder prediction methods. *Proteins 65*, 1−14.
(66) Barbar, E. (1999) NMR characterization of partially folded and unfolded conformational ensembles of proteins. *Biopolymers 51*, 191−207.
(67) Dyson, H. J., and Wright, P. E. (1998) Equilibrium NMR studies of unfolded and partially folded proteins. *Nat. Struct. Biol.*, 499−503.
(68) Lise, S., and Jones, D. T. (2005) Sequence patterns associated with disordered regions in proteins. *Proteins 58*, 144−150.
(69) Radivojac, P., Iakoucheva, L. M., Oldfield, C. J., Obradovic, Z., Uversky, V. N., and Dunker, A. K. (2007) Intrinsic disorder and functional proteomics. *Biophys. J. 92*, 1439−1456.
(70) Katz, C., Levy-Beladev, L., Rotem-Bamberger, S., Rito, T., Rudiger, S. G., and Friedler, A. (2011) Studying protein−protein interactions using peptide arrays. *Chem. Soc. Rev. 40*, 2131−2145.

DOI: 10.1021/acs.biochem.5b00084
Biochemistry 2015, 54, 3337−3347